



One-shot absolute pattern for dense reconstruction using DeBruijn coding and Windowed Fourier Transform

Sergio Fernandez*, Joaquim Salvi

Institute of Informatics and Applications, University of Girona, Av. Lluís Santalo S/N, E-17071 Girona, Spain

ARTICLE INFO

Article history:

Received 22 May 2012

Received in revised form

4 October 2012

Accepted 8 October 2012

Available online 15 November 2012

Keywords:

Structured light

Windowed Fourier transform

Fringe analysis

DeBruijn pattern

Active stereo

Computer vision

ABSTRACT

Shape reconstruction using coded structured light (SL) is considered one of the most reliable techniques to recover object surfaces. Among SL techniques, the achievement of dense acquisition for moving scenarios constitutes an active field of research. A common solution is to project a single one-shot fringe pattern, extracting depth from the phase deviation of the imaged pattern. However, the algorithms employed to unwrap the phase are computationally slow and can fail in the presence of depth discontinuities and occlusions. In this work, a proposal for a new one-shot dense pattern that combines DeBruijn and Windowed Fourier Transform to obtain a dense, absolute, accurate and computationally fast 3D reconstruction is presented and compared with other existing techniques.

© 2012 Elsevier B.V. All rights reserved.

1. Introduction

Three dimensional measurement constitutes an important topic in computer vision applied in range sensing, industrial inspection of manufactured parts, reverse engineering (digitization of free-form surfaces), object recognition, 3D map building, biometrics, clothing design and others. Traditionally, measuring systems are classified into contact and non-contact according to whether the measuring surface is touched to perform the measurement, which represents a constraint in many applications. Non-contact measuring systems are subdivided into passive and active, depending on whether an additional and structured source of light is used in the measurement [1]. Active methods based on Structured Light (SL) are composed of a digital camera (or cameras) and a Digital Light Projector (DLP). DLP projects a designed pattern to impose the illusion of texture onto the measuring surface, increasing the number of correspondences [2], thus being able to perform measurements even in presence of textureless surfaces. Among SL techniques, one-shot patterns have the ability to measure moving surfaces (up to the acquisition time required by the camera). For instance, spatial multiplexing patterns perform one-shot 3D absolute reconstruction with good accuracy at the expense of acquiring a sparse (feature wise) measurement. This is the case of DeBruijn patterns, that create

a non-repetitive sequence of colored lines [3–5]; M-arrays patterns, that apply the same principle in the two coding axes [6–8]; or non-formal coding like Koninckx and Van Gool [9], where vertical stripes and diagonal crossing lines define epipolar-constrained unique crossing points. Besides, one-shot fringe-based patterns achieve dense (pixel wise) reconstruction. However, inaccuracies can occur at surface discontinuities due to the non-absolute (periodic) coding intrinsic to the method [10]. Despite some solutions like the one proposed by Sitnik [11] minimize its probability, still discontinuity errors can occur when a single frame is projected. There exist some techniques that obtain density and absolute coding by using one-shot spatial grading [12,13], but both achieve a rather low accuracy [10]. Therefore, the problem of designing a one-shot-based pattern providing dense measurement, absolute coding and high accuracy still remains unsolved.

This work presents a new one-shot pattern for 3D dense reconstruction. The main idea is to combine the benefits of DeBruijn coding in dense fringe-based patterns using the Windowed Fourier Transform (WFT) analysis, with the goal of obtaining from a unique image an absolute, accurate and computationally fast 3D reconstruction. The paper is structured as follows: Section 2 presents a brief overview of one-shot dense acquisition techniques. Section 3 presents the design of the new technique especially focused on the absolute coding unwrapping. Experimental results with both simulated and real data are presented in Section 4, including a comparison with other existing SL techniques. Finally, Section 5 concludes with a discussion of the proposed method,

* Corresponding author.

E-mail addresses: sergiofn@eia.udg.edu (S. Fernandez), qsalvi@eia.udg.edu (J. Salvi).

analyzing its advantages and disadvantages compared to the literature.

2. A brief overview of one-shot dense acquisition techniques

There exist some techniques that perform dense (pixel-wise) reconstruction by projecting a unique (one-shot) pattern. Two main groups can be distinguished regarding the classification of Salvi et al. [10]: spatial grading and frequency multiplexing. Both of them show a continuous variation in intensity or color throughout one or both pattern axes. In grading methods the entire codeword for a given pixel position is stored in the pixel (gray level or color). Grayscale-based patterns [12] and color-based patterns [13] are found in the literature. However, both suffer of high sensitivity to signal noise due to the short distance between codewords of adjacent pixels. In frequency multiplexing, depth extraction is performed in the frequency domain rather than in the spatial domain. Fourier Transform, Windowed Fourier Transform and Wavelet Transform techniques have been traditionally used for this purpose.

Fourier Transform (FT) was introduced to solve the necessity of having a phase-shifting-based method for moving surfaces. FT was first proposed by Takeda and Mutoh [14], who extracted depth from one single projected pattern. A sinusoidal grating was projected onto the measuring surface, and the reflected deformed pattern was recorded. The projected signal for a sinusoidal grating was represented as

$$I_n^p(y^p) = A^p + B^p \cos(2\pi f_\phi y^p) \quad (1)$$

Once reflected, the phase component is modified by the shape of the surface. Note that the phase component must be isolated to extract shape information. This was achieved performing a frequency filtering in the Fourier domain. The background component was suppressed and a translation in frequency was done to bring the carrier component (which holds the phase information) to zero frequency axis. To extract the phase, the input signal was rewritten as

$$I(x,y) = a(x,y) + c(x,y)e^{2\pi i f_\phi y^p} + c^*(x,y)e^{-2\pi i f_\phi y^p} \quad (2)$$

where

$$c(x,y) = \frac{1}{2}b(x,y)e^{i\phi(x,y)} \quad (3)$$

where $c^*(x,y)$ is the complex value of constant $c(x,y)$. Finally, the phase component was extracted from the imaginary part of the following equation:

$$\log[c(x,y)] = \log\left[\frac{1}{2}b(x,y)\right] + i\phi \quad (4)$$

The obtained phase component ranges from $(-\pi, \pi]$, being necessary to apply an unwrapping algorithm in order to obtain a continuous phase related to the object. Once the phase was unwrapped, the relative depth information was extracted using the following equation:

$$h(x,y) = L \cdot \frac{\Delta\phi(x,y)}{(\Delta\phi(x,y) - 2\pi f_0 d)} \quad (5)$$

where L is the distance to the reference plane and d is the distance between the camera and the projector devices. However, due to the periodic nature of the projected pattern, this method is constrained by the maximum slope that can be reconstructed given by

$$\left| \frac{\partial h(x,y)}{\partial x} \right|_{MAX} < \frac{L}{3d} \quad (6)$$

The *Windowed Fourier Transform* (WFT) splits the signal into segments before the analysis in frequency domain is performed,

reducing the frequency overlapping between background and data. These segments must be small enough to reduce the errors introduced by boundaries, holes and background illumination, at the same time it must be big enough to hold some periods and hence allow the detection of the main frequency to perform an optimal filtering (this tradeoff was evaluated in the work of [15]). The received signal is filtered applying the WFT analysis transform shown in

$$Sf(u,v,\xi,\eta) = \int_{-\infty}^{\infty} \int_{-\infty}^{\infty} f(x,y) \cdot g(x-u,y-v) \cdot \exp(-j\xi x - j\eta y) dx dy \quad (7)$$

being (x,y) , (ξ,η) the translation and frequency coordinates respectively, and $g(x,y)$ the windowing function. When $g(x,y)$ is a gaussian window, the WFT is called a Gabor transform. Eq. (7) provides the 4-D coefficients $Sf(u,v,\xi,\eta)$ corresponding to the 2D input image. The next step is to apply one of the two phase extraction algorithms: Windowed Fourier Filtering (WFF) and Windowed Fourier Ridge (WFR) [16]. In WFF the 4D coefficients are first filtered, suppressing the small coefficients (in terms of its amplitude) that correspond to noise effects. The inverse WFT is then applied to obtain a smooth image, and the estimated frequencies $\omega_x(x,y)$ and $\omega_y(x,y)$ and their corresponding phase distributions are obtained from the angle given by the filtered WFF, as explained in [17]. In WFR, however, the estimated frequencies are extracted from the maximum of the spectrum amplitude, as shown in the following equation:

$$[\omega_x(u,v), \omega_y(u,v)] = \operatorname{argmax}_{\xi,\eta} |Sf(u,v,\xi,\eta)| \quad (8)$$

The phase can be directly obtained from the angle of the spectrum for those frequency values selected by the WFR (phase from ridges), or integrating the frequencies (phase by integration).

Wavelet Transform (WT) is another windowed based approach, where the window size increases when the frequency decreases, and vice-versa. This permits to remove the background illumination and prevent the propagation of errors produced during the analysis, which remain confined in the corrupted regions [16]. Additionally the leakage effects are reduced, avoiding large errors at the edges of the extracted phase maps. The Continuous Wavelet Transform (CWT) is a sub-family of WT that performs the transformation in the continuous domain [18]. Similar to WFT, in 2D analysis a 4D transform is obtained from WT (the daughter wavelets are obtained by translation, dilation and rotation of the previously selected mother wavelet). Once this is performed, phase extraction is pursued using the phase from ridges or the phase by integration algorithms. It is important to mention that in WT the window size increases when the horizontal or vertical fringe frequencies decreases. This can be a troublesome for the analysis of some fringe patterns where the carrier frequency is extremely low or high, as was pointed out by Kemao et al. [19]. Moreover, in computational applications a dyadic net is used to generate the set of wavelet functions (that is, the size of the wavelet is modified by the factor 2^j). This can be a drawback for fringe pattern analysis, where the change in the spatial fringe frequencies throughout the image is not high enough to produce a relative variance of 2^j in the size of the optimal wavelet.

3. A new proposal for one-shot dense reconstruction

The proposed technique combines the accuracy of DeBruijn slit-based patterns with the density of fringe WFT-based patterns, in a unique (one-shot) pattern. One-shot projection allows the algorithm to reconstruct moving surfaces, or to be used for a post-

processing 3D retrieval of a dynamic environment (real-time processing is not considered in this work). A general scheme of the algorithm is shown in Fig. 1 and explained in the following lines.

3.1. Camera–projector calibration

The camera–projector calibration was done using the algorithm of Fernandez et al. [20], which models the projector as the inverse of a pinhole camera. First, the camera is calibrated using the Bouguet's implementation of the Zhang's technique [21]. Afterwards, a calibration image (a checkerboard) is projected onto a plane and captured by the camera. The 3D coordinates of

this plane are found using some fixed and marked positions on the plane (see Fig. 2). Therefore, 3D coordinates of the projected checkerboard points are found using the camera parameters. Finally, projector calibration is performed using these 3D points and the same calibration procedure employed for the camera.

3.2. Pattern creation

The proposed pattern consists on a colored sinusoidal fringe pattern, where the color of the different fringes follows a DeBruijn sequence. DeBruijn sequences are a set of pseudorandom values having specific properties between them. This prevents from decoding errors that may arise in non-coded color fringe patterns proposals [22]. A k -ary DeBruijn sequence of order n is a circular sequence $d_0, d_1, \dots, d_{n^k-1}$ (length n^k) containing each substring of length k exactly once (window property of k). DeBruijn sequences can be constructed directly from the Hamiltonian or Eulerian path of a n -dimensional DeBruijn graph (see [23] for more details). In our approach we set $n=3$ as we work only with red, green and blue colors. Moreover, we set the pattern to have 64 fringes—this is a convention given the pixel resolution of the projector and the camera. Therefore, $n^k \geq 64$, so we set the window property to $k=4$. An algorithm performing the sequence generation provides us an arbitrary DeBruijn circular sequence d_0, d_1, \dots, d_{80} . The pattern, of size $m \times n$, is generated in the HSV space. For every column $j = 1..m$ of the V channel, the sinusoidal signal is represented as

$$I(i, j) = 0.5 + 0.5 \cdot \cos(2\pi fi) \quad (9)$$

where $i = 1..n$ and the discrete frequency $f = 64/n$.

The H channel maps a value of the previously computed DeBruijn sequence to every period of the V channel. The S channel is set to 1 for all the pixels to obtain the maxima of the saturation value. Finally, the created HSV matrix is transformed into RGB values. The resulting pattern is shown in Fig. 3.

3.3. Color calibration

A color calibration reveals necessary to extract the three different projected colors from the acquired image. To this end, Caspi et al. [24], developed a color calibration algorithm based on linearizing the projector-camera matrix and the surface reflectance matrix, specific for every scene point projected into a camera pixel. Our proposal considers a modification of this techniques, where a global and unique transformation matrix is computed. A Least-Squares algorithm is applied to extract the linear estimated transformation matrix. This is done for each position and for each recovered channel. An example of the projected and recovered values for an arbitrary non-calibrated pixel is shown in Fig. 4. As can be observed, crosstalk (specially in the green channel) and surface albedo are present in the retrieved color values. Moreover, the DeBruijn vocabulary was minimized up to three colors, in order to maximize the Hamming distance present in the Hue channel and thus minimize the effect of crosstalk that may remain after color calibration (Fig. 5).

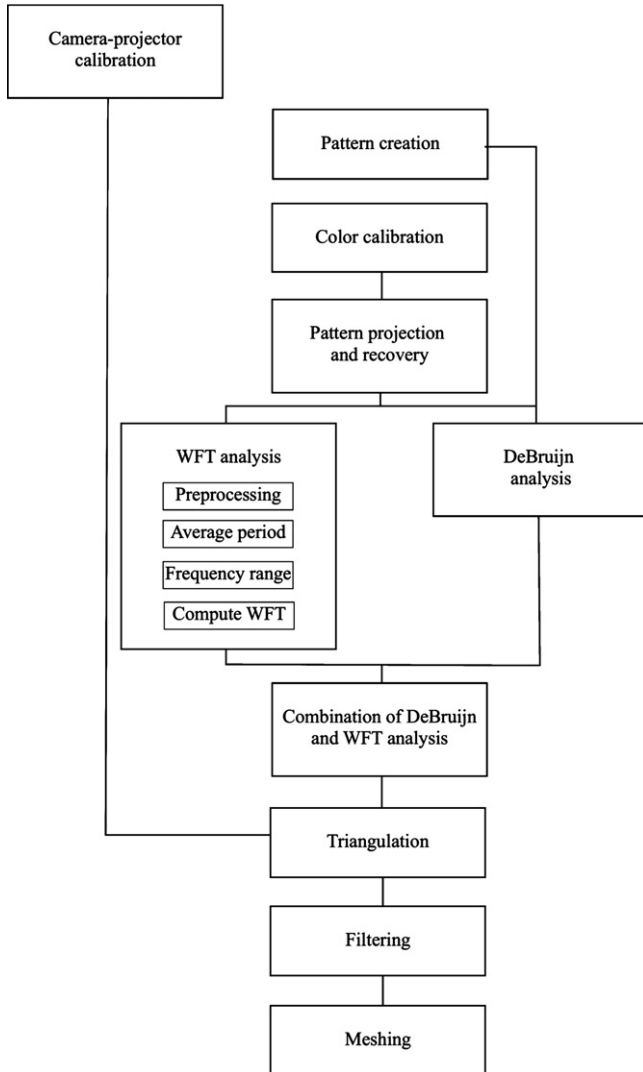


Fig. 1. Diagram of the proposed algorithm.

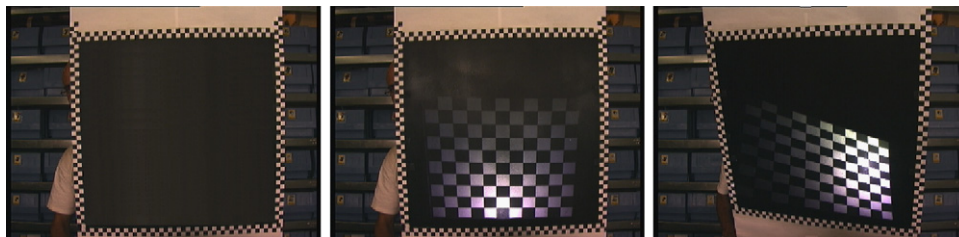


Fig. 2. Images showing the calibration plane (left) and two checkerboard projections at different positions.

3.4. Pattern projection and recovery

The designed pattern is projected by the active device. Once reflected onto the object, the pattern is recovered by the camera. The camera calibration matrix is applied to the RGB image, obtaining the corrected color values. The corrected RGB image is transformed to the HSV space. Afterwards, a Region Of Interest (ROI) is selected regarding the information held in the V plane. To this end, a closure morphological operation is applied followed by a binarization. Those pixels exceeding the value given by the Otsu thresholding algorithm are selected for the ROI. Finally, the ROI is applied to the corrected RGB image and to the V matrix. The RGB image is the input of the DeBruijn detection algorithm, whereas the V matrix is used in the Windowed Fourier Transform Analysis.

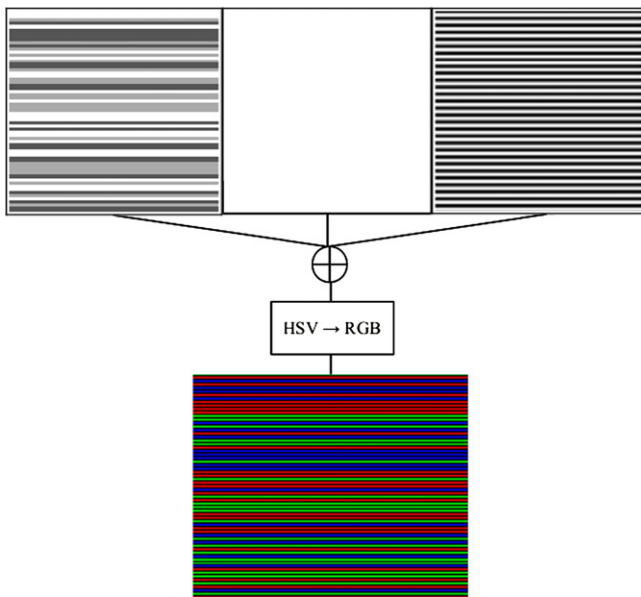


Fig. 3. Proposed pattern: HSV representation of the DeBruijn sequence (top-left), fringe pattern (top-right) and the resulting RGB pattern for $m=64$ (bottom).

3.5. DeBruijn analysis

The aim of this step is to extract the color associated to every deformed colored fringe. We followed the same approach used in slit-based pattern, provided the recovered fringes present a gaussian-like shape similar to that present in slit-based patterns [1,10]. Therefore, a maxima localization algorithm is applied searching local maxima (detected with sub-pixel precision) on every color channel of the current scan-column. The implemented algorithm takes into account the total of $n=64$ periods present in the pattern, and the consecutive maxima-minima distribution. Furthermore, a global threshold suppressing peaks lower than the 70% of maximum peak is applied. These steps prevent from false peaks detection.

Dynamic programming. Ideally, the matching of correspondences between the projected sequence and the perceived one is straightforward. However, usually the whole sequence of projected stripes is not visible in the image scan-line or some of them are incorrectly labeled or disorders may occur. Therefore, the use of dynamic programming becomes compulsory. Dynamic programming works as a scoring function, measuring the similarities between the projected and the recovered color sequences (see [5] for more details).

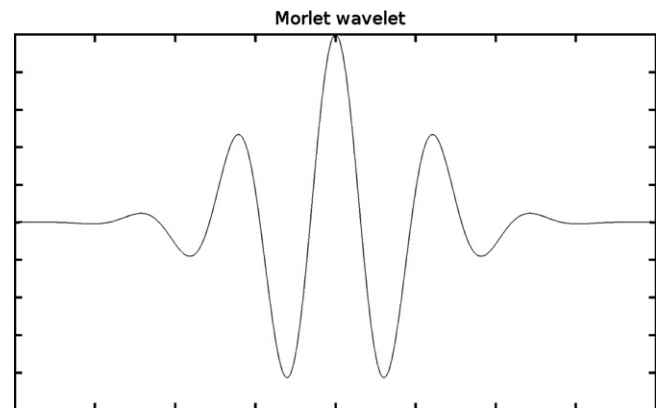


Fig. 5. Visual representation of a Morlet signal with $n=3$ periods.

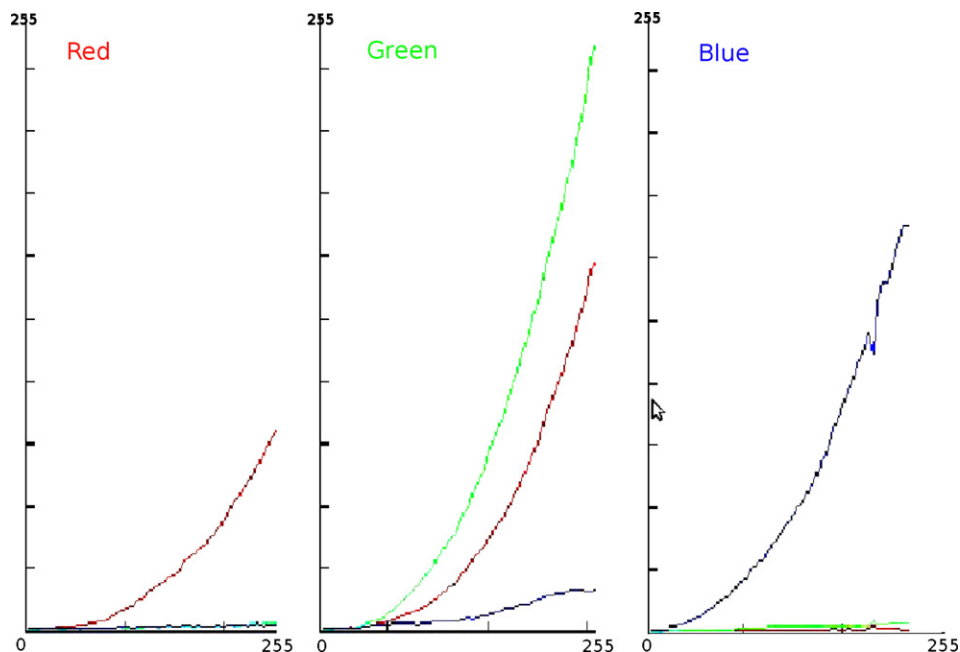


Fig. 4. Received color intensities for uniformly increasing values of red, green and blue, respectively. (For interpretation of the references to color in this figure caption, the reader is referred to the web version of this article.)

3.6. Windowed Fourier Transform analysis

The WFT has been chosen for frequency fringes analysis, as it prevents from leakage distortion. Moreover, it has a more precise window width selection than WT. First, a salt and pepper filtering and a histogram equalization is applied to the V channel. Afterwards, an adapted Morlet wavelet is chosen for WFT analysis. Regarding the work of Fernandez et al. [15], this provides good frequency and spatial localization at the same time. Morlet signal definition is

$$\Psi_{\text{Morlet}}(x) = \frac{1}{(f_c^2 \pi)^{1/4}} \exp(2\pi i f_c x) \cdot \exp\left(\frac{-x^2}{2f_b^2}\right) \quad (10)$$

where f_c is the mother wavelet central frequency and f_b is the window size.

The average and standard deviation of the fringe period is estimated counting the number of periods existing in every column along the coding axis (using the same algorithm employed to find the local maxima of the DeBruijn sequence). Average period (pm) and standard deviation (std) are extracted from the single periods corresponding to each column. The std represents the uncertainty in the estimated frequency, and is crucial to perform a global analysis of the image. The average frequency for the $n \times m$ pattern is computed as $f_m = n/pm$. The frequencies analyzed are in the range $[f_m - 3 \cdot std, f_m + 3 \cdot std]$ in both x and y axes, where f_m is the average frequency. Using this range the 99% of detected frequencies are analyzed. In practice, this range can be reduced to $[f_m - 2 \cdot std, f_m + 2 \cdot std]$ (95% of the frequencies are represented) without a significant lose in accuracy. Another variable to consider is the window size related to the number of periods of the sinusoidal mother signal. In contrast to the mother wavelets in WT, WFT does not require the number of periods to be linked to the sinusoidal oscillation of the signal. In our algorithm it has been used from one up to three periods. The optimal value is selected applying the ridge extraction algorithm (WFR), which computes the most likely values of window (w_x, w_y) and the corresponding phase value. finally, the wrapped phase in the interval $[-\pi, \pi]$ is obtained.

3.7. Combination of DeBruijn and wrapped phase patterns

The next step is to merge the information obtained from the WFT and the DeBruijn algorithms. The wrapped phase is merged with the extracted colored lines. Due to the 2D nature of the WFT

algorithm (which may include some frequencies of adjacent positions in the Fourier Transform) the phase value of a specific position may have some deviation. This effect is corrected shrinking or expanding the wrapped phase accordingly to the DeBruijn correspondences for the maxima. A nonlinear fourth order regression line is used to this end, matching the maxima of the wrapped phase map with the position of the colored lines in the DeBruijn map. This process is done for every column in the image, obtaining corrected wrapped phase map. This is shown in Fig. 6. Finally, the correspondence map provided by the DeBruijn lines is expanded using the wrapped phase map. The phase values between two adjacent lines go in the range $(-\pi, \pi)$. Therefore, a direct correlation is set between these values and the position of the projected and the recovered color intensities. A full (dense) correspondences map is obtained.

3.8. 3D recovering and filtering

The previously extracted full correspondences map is given to the triangulation algorithm. Using the extrinsic and intrinsic parameters of the camera–projector system, a tri-dimensional cloud of points in (x,y,z) is computed, representing the shape of the reconstructed surface. A posterior filtering step reveals necessary due to some erroneous matchings that originate outliers in the 3D cloud of points. To this end, two different filtering steps are applied.

3D statistical filtering. In the 3D space, the outliers are characterized by their extremely different 3D coordinates regarding the surrounding points. Therefore, pixels having 3D coordinates different than the 95% of the coordinates of all the points are considered for suppression. This is done in two steps for all the points in the 3D cloud. First the distance to the centroid of the cloud is computed, for every pixel. Afterwards, those pixel having a distance to the centroid greater than two times the standard deviation of the cloud of points are considered as outliers.

Bilateral filtering. Still, there can be some misaligned points after applying the statistical filtering. In this case it would be profitous to apply some anisotropic filtering that filters the data while preserving the slopes. To this end, an extension to 3D data of the 2D bilateral filter proposed by Tomati and Manduchi [25] was implemented. The bilateral filter is a non-recursive anisotropic filter whose aim is to smooth the cloud of points (up to a given value) while preserving the discontinuities, by means of a nonlinear combination of nearby point values. The proposed 3D

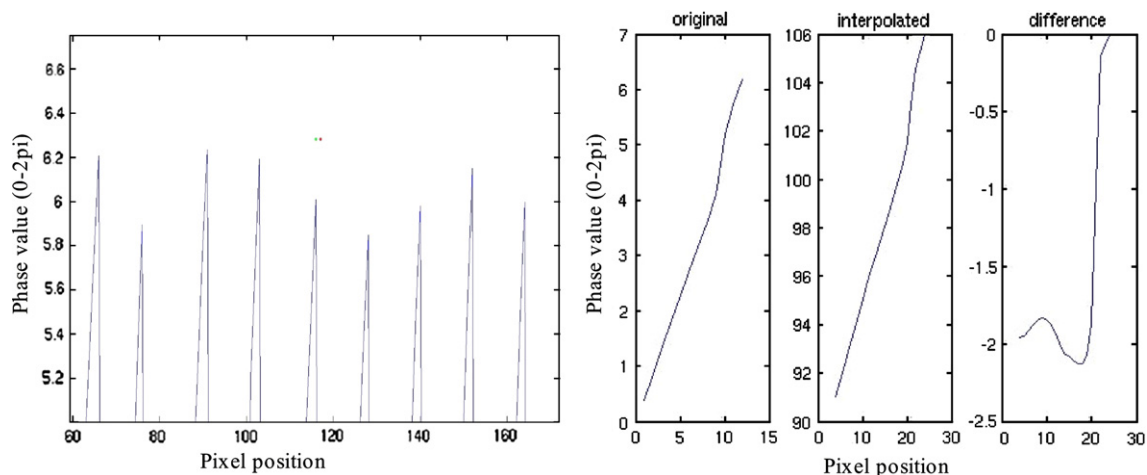


Fig. 6. On the left, detail of the wrapped phase and a crest maxima (in red), and its corresponding slits line position (in green). On the right, the wrapped section before and after correction, and the correction interpolation error. (For interpretation of the references to color in this figure caption, the reader is referred to the web version of this article.)

bilateral filtering is described as

$$G(x,y) = \exp(-((x-x_c)^2 + (y-y_c)^2)/(2*\sigma_1^2)) \tag{11}$$

$$H(z) = \exp(-(z-z_c)^2/(2*\sigma_2^2)) \tag{12}$$

where x,y,z are the 3D coordinates of a given point, $G(x,y)$ is the distance mask, $H(z)$ is the height mask, and both σ_1 and σ_2 are values to set empirically. The algorithm works as follows: given a set of points X,Y,Z around the selected 3D point, the corresponding masks $G(x,y)$ and $H(z)$ are computed, providing the filtered results. This modified the height of those isolated pixels having a 3D coordinates much different than their vicinity, while preserving the slopes.

4. Results

The proposed algorithm was implemented and tested in both simulated and real data. Moreover, a comparison with other representative SL algorithms was pursued. To this end we used the techniques present in the work of Salvi et al. [10]. They correspond to the main groups existing in SL, not only in dense but also sparse reconstruction. The setup used for the tests was composed of an DLP video projector (Epson EMP-400W) with a resolution of 1024×768 pixels, a camera (Sony 3 CCD) and a frame grabber (Matrox Meteor-II) digitizing images at 768×576 pixels with 3×8 bits per pixel (RGB). The baseline between camera and projector was about 60 cm. Experiments were computed in a desktop computer, Intel Core2 Duo CPU at 3.00 GHz and 4 GB RAM memory. The algorithms were programmed and ran in Matlab 7.3. It is important to mention the methods used for comparison were re-programmed from the corresponding papers, since at the best of our knowledge source codes were not available.

4.1. Simulation results

The *peaks* function available in Matlab (shown in Fig. 7) has become a benchmark for 3D reconstruction in SL, specially in fringe pattern analysis, as stated in [10]. A noised version with gaussian random noise having zero mean and standard deviation of 0.05%, 0.1%, 0.15% and 0.2% was reconstructed and compared with the input. Moreover, a comparison with the other one-shot techniques selected in [10] was done. The results are shown in Fig. 8.

As can be observed, the algorithm of Carrhill and Hummel performs the worst, due to the high sensitivity to signal noise caused by the short distance between codewords of adjacent pixels. Su et al. algorithm performs optimally for low noise values thanks to the nature of the 2D frequency analysis, which smoothes the incoming data. This occurs also for the proposed

pattern. However, for noised images having $std > 0.1$ the 1D unwrapping step of Su et al. introduces discontinuities in the recovered phase, leading to errors in the pixel position. Besides, Monks algorithm suffers the low amount of reconstructed points, which penalizes the errors produced in the slits position. Finally, the proposed algorithm provides a much denser reconstruction with 2D fourier analysis and no need to perform any phase unwrapping. This fact is reflected in the results, performing the best among the three tested techniques.

4.2. Empirical results

Quantitative results were analyzed reconstructing a white plane at a distance of about 80 cm in front of the camera. Principle Component Analysis (PCA) was applied to obtain the equation of

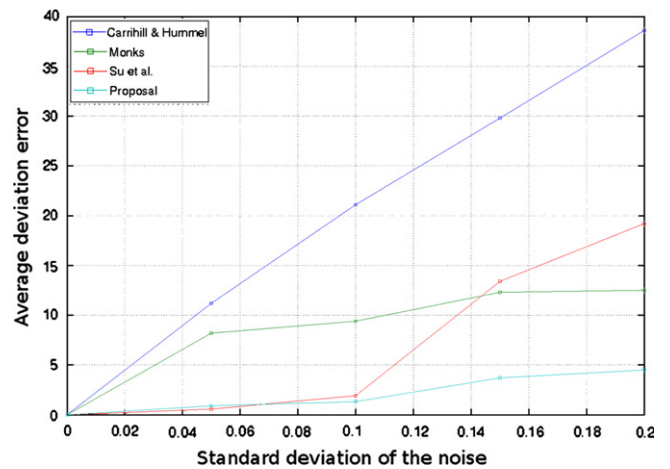


Fig. 8. Normalized error on reconstructed depth positions for different values of noise.

Table 1

Quantitative results. The headings are: author's name of the technique, average deviation of the reconstructing error, standard deviation of the reconstructing error, number of 3D points reconstructed, and number of projected patterns.

Technique	Average (mm)	Stdev (mm)	3D points	Patterns
Monks et al.	1.31	1.19	13,899	1
Posdamer et al.	1.56	1.40	25,387	14
Guhring	1.52	1.33	315,273	24
Pribanic et al.	1.12	0.78	255,572	18
Carrhill and Hummel	11.9	5.02	202,714	1
Proposed technique	1.18	1.44	357,200	1

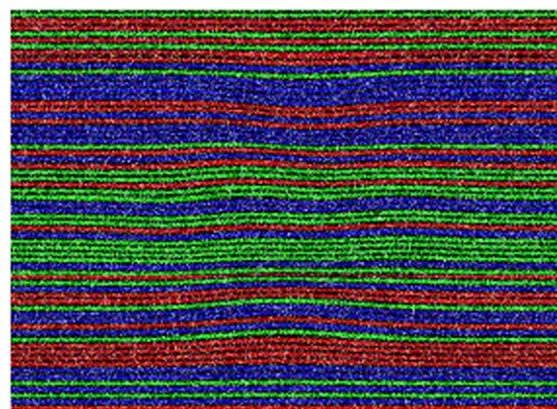
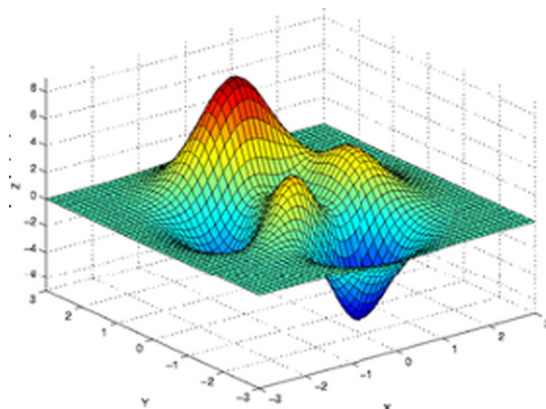


Fig. 7. Peaks signal and recovered pattern for the proposed algorithm and noise of $std=0.1$.

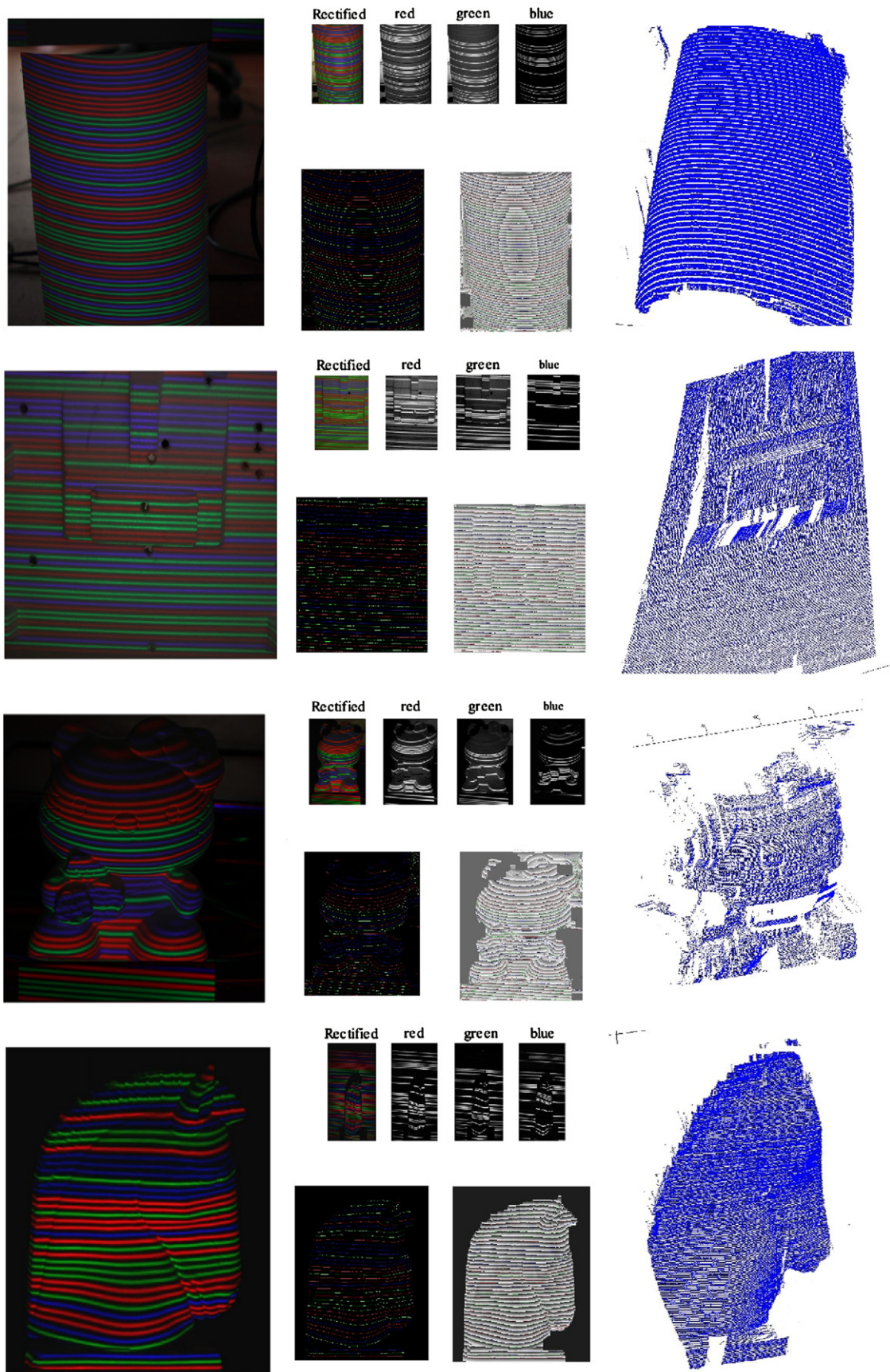


Fig. 9. For every object: on the left, input image. On the center the rectified extracted colors channels, and the slits and fringes patterns. On the right the recovered 3D cloud of points.

the 3D plane for every technique and for every reconstruction. PCA is used to span the 3D cloud of points onto a 2D plane defined by the two eigenvectors corresponding to the two largest eigenvalues. The results of the experiment are shown in Table 1.

Note that the algorithm of Su et al. [26] is conceived to measure deviation of smooth surfaces with respect to the reference plane, therefore a plane is not conceived to be reconstructed by depth deviation. As can be observed, the proposed technique obtains one of the best accuracy results in terms of average and

standard deviation of the error, only overcome by the method of Pribanic et al. [27], which requires a total of 18 projected patterns. Among the one-shot projection techniques, the proposed technique obtains the best accuracy results jointly with another DeBruijn based technique, the sparse reconstruction algorithm proposed by Monks et al. [3]. Regarding the computing time it can be observed that methods obtaining dense reconstructions (the case of Guhring, Pribanic et al., Su et al., and Carrhill and Hummel and the proposed algorithm) need to compute more 3D

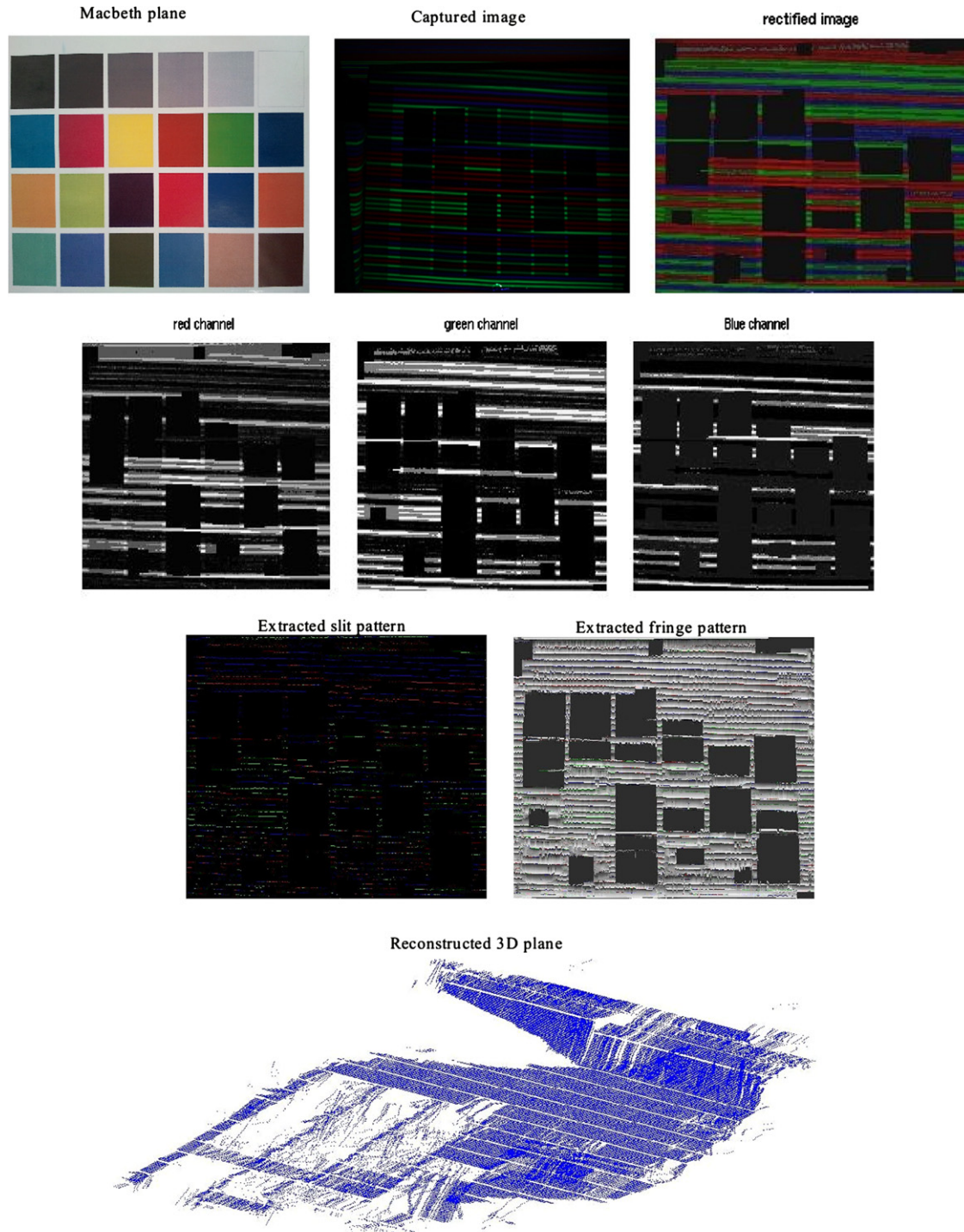


Fig. 10. 3D retrieval of a Macbeth checker plane. 1st row: original and color rectified image. 2nd row: RGB channels before DeBruijn and WFT analysis. 3rd row: extracted DeBruijn color slits and WFT wrapped phase. 4th row: retrieved 3D plane. (For interpretation of the references to color in this figure caption, the reader is referred to the web version of this article.)

points, requiring higher computational time. However, our proposal does not need to compute many images, nor any unwrapping algorithm is required. This makes our technique faster in terms of computational time. Among methods providing sparse reconstruction the color calibration step makes Monks et al. algorithm slower than Posdamer et al. (also affects the proposed technique) despite it preserves the same order of magnitude. Still, real time response is achievable working with the appropriate programming language and firmware.

Finally, *Qualitative results* were pursued reconstructing several 3D objects. The lambertian objects were placed at a distance of about 80 cm to the camera. Results of 3D reconstruction are shown in Fig. 9. The first reconstruction corresponds to a bended piece of sheet. The second reconstruction is a piece of manufactured cork. Third and fourth reconstructions are ceramic figures of a 'hello kitty' and a horse, respectively. As can be observed the objects are reconstructed optimally. Only the 'hello kitty' present some points missing, as the filtering suppressed 3D outliers associated to the low illuminated and blurred regions present in the recovered image.

Moreover, a test on color resistance was pursued. When projecting onto a color surface, the color of the fringes get distorted by the original color of the object. Therefore, the identification of the color sequence by the DeBruijn decoding algorithm may present some errors. This phenomena has been tested for a real colored object. The aim was to reconstruct a planar surface having different colors, in different positions not related with the orientation of the fringes. A Macbeth color-checker with 24 different colors, originally proposed by McCamy et al. [28], was used to this end. The results of scanning and 3D reconstruction are shown in Fig. 10.

As can be observed, the reconstruction fails in dark regions, as the reflected illumination is not high enough to detect the fringe colors in the DeBruijn algorithm. This causes big holes in the reconstruction after the filtering is applied. However, the structure of the plane in the bright color areas is preserved.

5. Conclusion

This paper proposes a new technique for one-shot dense 3D surface reconstruction, which combines the accuracy of DeBruijn spatial multiplexing with the density of frequency multiplexing in fringe projection. One-shot projection allows the algorithm to reconstruct moving objects, or to be used for a post-processing 3D retrieval of a dynamic environment. The proposal has been implemented and compared both quantitatively and qualitatively with some representative techniques of Structured Light. Simulation results and empirical quantitative results show the good performance of the proposed technique in terms of resistance to noise and accuracy of a reconstructed plane. Among the compared techniques, the proposed method is only overcome by the time multiplexing shifting approach proposed by Pribanic et al. [27], which is only valid for static scenarios. Among one-shot techniques, our proposed method achieves the best results in terms of accuracy, comparable with other DeBruijn-based spatial coding. Moreover, dense reconstruction and absolute coding is assured with the proposed technique. Besides, other frequency multiplexing methods provide dense reconstruction for moving scenarios, but present high sensitivity to details in the surface, and can fail under presence of big slopes. Finally, 3D reconstruction of some real objects has been pursued. For lambertian surfaces the algorithm works effectively in terms of density and perceived quality of the one-shot reconstruction. For colored surfaces, the algorithm still works under colored bright regions but fails under dark regions. Most of the works presented in SL during last years have been concerned into frequency multiplexing approaches,

trying to increase the robustness in the decoding step and the resistance to slopes under the constraint of moving scenarios [29,16]. Under this scenario, the proposal made in this work of merging DeBruijn and frequency-based one-shot patterns achieves a dense reconstruction with the robustness in the decoding step provided by frequency analysis, jointly with the accuracy given by spatial DeBruijn-based patterns. This combination gives us an accurate one-shot absolute dense pattern able to work in moving scenarios.

Acknowledgments

This work has been partly supported by the FP7-ICT-2011-7 project PANDORA—Persistent Autonomy through Learning, Adaptation, Observation and Re-planning (Ref 288273) funded by the European Commission and the project RAIMON—Autonomous Underwater Robot for Marine Fish Farms Inspection and Monitoring (Ref CTM2011-29691-C02-02) funded by the Spanish Ministry of Science and Innovation. S. Fernandez is supported by the Spanish government scholarship FPU.

References

- [1] J. Batlle, E. Mouaddib, J. Salvi, *Pattern Recognition* 31 (7) (1998) 963.
- [2] J. Salvi, J. Pages, J. Batlle, *Pattern Recognition* 37 (4) (2004) 827.
- [3] T. Monks, J. Carter, C. Shadle, Colour-encoded structured light for digitisation of real-time 3D data, in: *IEE 4th International Conference on Image Processing*, 1992, pp. 327–330.
- [4] J. Pages, J. Salvi, C. Collewet, J. Forest, *Image Vision and Computing* 23 (2005) 707.
- [5] L. Zhang, B. Curless, S. Seitz, Rapid shape acquisition using color structured light and multi-pass dynamic programming, in: *3D Data Processing Visualization and Transmission*, 2002, pp. 24–36.
- [6] H. Morita, K. Yajima, S. Sakata, Reconstruction of surfaces of 3-d objects by m-array pattern projection method, in: *Second International Conference on Computer Vision*, 1988, pp. 468–473.
- [7] R. Morano, C. Ozturk, R. Conn, S. Dubin, S. Zietz, J. Nissano, *IEEE Transactions on Pattern Analysis and Machine Intelligence* 20 (3) (1998) 322.
- [8] J. Pages, C. Collewet, F. Chaumette, J. Salvi, S. Girona, F. Rennes, An approach to visual servoing based on coded light, in: *IEEE International Conference on Robotics and Automation, ICRA*, vol. 6, 2006, pp. 4118–4123.
- [9] T. Koninckx, L. Van Gool, *IEEE Transactions on Pattern Analysis and Machine Intelligence* 28 (3) (2006) 432.
- [10] J. Salvi, S. Fernandez, T. Pribanic, X. Llado, *Pattern Recognition* 43 (8) (2010) 2666.
- [11] R. Sitnik, *Applied Optics* 48 (18) (2009) 3344.
- [12] B. Carrhill, R. Hummel, *Computer Vision, Graphics, and Image Processing* 32 (3) (1985) 337.
- [13] J. Tajima, M. Iwakawa, 3-D data acquisition by rainbow range finder, in: *Proceedings of the 10th International Conference on Pattern Recognition*, vol. 1, 1990, pp. 309–313.
- [14] M. Takeda, M. Mutoh, *Applied Optics* 22 (1983) 3977.
- [15] S. Fernandez, M.A. Gdeisat, J. Salvi, D. Burton, *Optics Communications* 284 (12) (2011) 2797.
- [16] M. Gdeisat, D. Burton, M. Lalor, *Optics Communications* 266 (2) (2006) 482.
- [17] Q. Kema, *Optics and Lasers in Engineering* 45 (2) (2007) 304.
- [18] A.Z.A. Abid, Fringe Pattern Analysis Using Wavelet Transforms, Ph.D. Thesis, General Engineering Research Institute (GERI), Liverpool John Moores University, Liverpool, UK, 2008.
- [19] Q. Kema, *Applied Optics* 43 (17) (2004) 3472.
- [20] Sergio Fernandez, Joaquim Salvi, Planar-based camera-projector calibration, in: *Proceedings of the IEEE 7th International Symposium on Image and Signal Processing and Analysis (ISPA 2011)*, Dubrovnik (Croatia), September 4–6, 2011.
- [21] X. Zhang, L. Zhu, *Optical Engineering* 48 (2009) 117208.
- [22] Y. Wang, S. Yang, X. Gou, *Optics Letters* 35 (5) (2010) 790.
- [23] H. Fredricksen, *SIAM Review* (1982) 195.
- [24] D. Caspi, N. Kiryati, J. Shamir, *IEEE Transactions on Pattern Analysis and Machine Intelligence* 20 (5) (1998) 470.
- [25] C. Tomasi, R. Manduchi, Bilateral filtering for gray and color images, in: *Sixth International Conference on Computer Vision, IEEE*, 1998, pp. 839–846.
- [26] J. Li, X. Su, L. Guo, *Optical Engineering* 29 (12) (1990) 1439.
- [27] T. Pribanic, H. Dapo, J. Salvi, Efficient and low-cost 3D structured light system based on a modified number-theoretic approach, *EURASIP Journal on Advances in Signal Processing* 2010, 2010:474389, <http://dx.doi.org/10.1155/2010/474389>.
- [28] C. McCamy, H. Marcus, J. Davidson, *Journal of Applied Photographic Engineering* 2 (3) (1976) 95.
- [29] W. Chen, P. Bu, S. Zheng, X. Su, *Optics and Laser Technology* 39 (4) (2007) 821.